Mutation of Murine Adenylate Kinase 7 Underlies a Primary Ciliary Dyskinesia Phenotype

Angeles Fernandez-Gonzalez[1,2], Stella Kourembanas[1,2], Todd A. Wyatt[3], and S. Alex Mitsialis[1,2]

[1]Division of Newborn Medicine, Children's Hospital Boston; [2]Department of Pediatrics, Harvard Medical School, Boston, Massachusetts; and [3]Pulmonary, Critical Care, Sleep Medicine and Allergy Section, Department of Internal Medicine, University of Nebraska Medical Center, Omaha, Nebraska

Primary ciliary dyskinesia (PCD) is a genetically and phenotypically heterogeneous disorder, characterized by progressive development of bronchiectasis, inflammation, and features characteristic of chronic obstructive pulmonary disease. We report here that a murine mutation of the evolutionarily conserved adenylate kinase 7 (Ak7) gene results in animals presenting with pathological signs characteristic of PCD, including ultrastructural ciliary defects and decreased ciliary beat frequency in respiratory epithelium. The mutation is associated with hydrocephalus, abnormal spermatogenesis, mucus accumulation in paranasal passages, and a dramatic respiratory pathology upon allergen challenge. Ak7 appears to be a marker for cilia with (9 + 2) microtubular organization. This is suggested by its tissue specificity of expression and also the stringent conservation of Ak7 ortholog structure only in protozoans and metazoans possessing motile (9 + 2) cilia. Collectively, our results indicate an ancestral and crucial role of Ak7 in maintaining ciliary structure and function, and suggest that mutations of the human ortholog may underlie a subset of genetically uncharacterized PCD cases.

Keywords: ciliopathies; airway epithelium; allergic inflammation; adenylate kinase; mouse model of disease

Primary ciliary dyskinesia (PCD) (OMIM 244400) is a congenital cause of recurrent respiratory disease, with an incidence of approximately 1 in 16,000 live births (1, 2). PCD is a genetically and phenotypically heterogeneous disorder, the underlying cause of which is the lack of effective ciliary motility due to abnormalities in the highly organized axoneme of cilia and sperm flagella (reviewed in Refs. 3, 4). Ciliary dysfunction in the respiratory epithelium causes impaired mucociliary clearance and precipitates chronic infection and inflammation of the upper and lower airways (5, 6). PCD cases are often associated with situs inversus, as in Kartagener syndrome, and rare cases may also present with hydrocephalus (7), retinitis pigmentosa (8, 9), and polycystic kidneys (10). A variety of ciliary ultrastructural defects have been associated with PCD, including absent or shortened dynein arms, defects in radial spokes, and ciliary microtubule transpositions. Mutations in members of the dynein gene family, *DNAI1* (11, 12), *DNAH5* (13, 14), and *DNAH11* (15), as well as mutations in the X-linked genes, *RPGR* (9, 16) and *OFD1* (17), have been recently implicated in the etiology of the disease, but the majority of PCD cases remain genetically uncharacterized.

CLINICAL RELEVANCE

The molecular characterization of a novel mouse model of primary ciliary dyskinesia impacts on research in asthma, allergy, and inflammation and could lead to the development of genetic diagnosis tools for a subset of primary ciliary dyskinesia cases.

In addition to structural integrity, proper ciliary function demands abundant energy. ATP hydrolysis is required not only to confer motility through the action of dynein ATPases, but also for transport of axonemal components necessary for elongation and maintenance of cilia and flagella (18, 19). A number of enzymatic relay mechanisms using ATP regeneration have been proposed to transport the high-energy phosphate from mitochondria along the length of the axoneme (20, 21). Members of the adenylate kinase (AK) family (EC2.7.4.3) have been postulated to provide an efficient way to relay energy to cellular compartments distal to sites of ATP production (22), and studies on flagellated protozoa (23, 24) have suggested an essential role of AK isoforms in ciliary function and homeostasis.

Animal models can be invaluable for our understanding of the molecular and physiologic basis of disease, and a number of gene ablation studies have targeted ciliary genes in the mouse (reviewed in 4). However, with the notable exceptions of mutants of the mouse ortholog of *DNAH5* (25) and of the less-well-characterized Dpcd locus (26), these animal models do not exhibit major respiratory pathology, the clinical hallmark of PCD. In this article, we characterize a mouse mutant presenting pathological signs characteristic of PCD, including high prevalence of microtubular defects, significantly decreased ciliary beat frequency, hydrocephalus, abnormal spermatogenesis, mucus accumulation in the paranasal passages, and exacerbated respiratory responses upon allergen challenge. We identified the underlying genetic lesion to be a mutation in the gene for Ak7, an atypical AK that appears to be a marker for motile (9 + 2) cilia.

MATERIALS AND METHODS

Ak7-Deficient Mice

All animal experimental protocols were approved by the Animal Care and Use Committee of the Children's Hospital Boston. The mutant mouse strain described here arose serendipitously in the process of generating transgenic mice harboring a tetracycline-regulatable heme oxygenase (HO)-1 construct, as detailed in the online supplement.

Allergen Sensitization and Challenge

Induction of chronic inflammation and airway remodeling was induced as previously described (27). Mice were immunized (intraperitoneally) on Days 1, 7, 14, and 21 with 25 μg of ovalbumin (OVA) (grade V; Sigma-Aldrich, St. Louis, MO) adsorbed to 1 mg of aluminum potassium sulfate

(*Received in original form March 14, 2008 and in final form August 11, 2008*)

This work was supported by National Institutes of Health SCOR grant HL67669 and R01 HL55454 (S.A.M. and S.K.), and by NIH grant R01 AA017993 (T.A.W.).

Correspondence and requests for reprints should be addressed to S. Alex Mitsialis, Ph.D., Division of Newborn Medicine, Enders 970, 300 Longwood Avenue, Children's Hospital Boston, Boston, MA 02115. E-mail: alex.mitsialis@childrens.harvard.edu

This article has an online supplement, which is accessible from this issue's table of contents at www.atsjournals.org

Am J Respir Cell Mol Biol Vol 40. pp 305–313, 2009
Originally Published in Press as DOI: 10.1165/rcmb.2008-0102OC on September 5, 2008
Internet address: www.atsjournals.org

dodecahydrate (alum; Sigma-Aldrich) in 200 μl of normal saline. Intranasal OVA challenges (20 ng/50 μl in 0.9% sodium chloride) were performed on Days 27, 29, and 31 under isoflurane anesthesia and then repeated twice a week for 1 month. Mice were harvested 24 hours after the final OVA challenge. For bronchoalveolar lavage fluid analysis, lungs were lavaged with 1 ml PBS and total white cell count was determined on Kimura-stained preparations using a hematocytometer chamber.

Northern Blot Analysis, RT-PCR, and Genomic PCR

Total tissue RNA was isolated using Qiagen RNeasy mini kits (Qiagen, Valencia, CA) and 1–2 μg was reverse transcribed using the Superscript first strand synthesis system for RT-PCR (Invitrogen Life Technologies, Carlsbad, CA). Genomic DNA was purified from brain using QIAam DNA kit (Qiagen) and amplified using Epicenter Biotechnologies Fail Safe System (Epicenter Biotechnologies, Madison, WI). Primers and conditions are detailed in the online supplementary MATERIALS AND METHODS.

Tissue Preparation

Mice were anesthetized with pentobarbital (60 mg/kg intraperitoneally) and perfused transcardially with 4% paraformaldehyde in 0.1 M phosphate buffer (pH 7.4). After perfusion, organs were removed and post-fixed for at least 4 hours in the same fixative. For histologic analysis of the lung, mice were perfused through the aorta with 0.1 M phosphate buffer (pH 7.4), and lungs were inflated with an intratracheal injection of 4% paraformaldehyde and post-fixed overnight at 4°C. Tissues were paraffin embedded and 5-μm-thick sections were cut on a microtome and mounted onto Fisherbrand Superfrost/Plus microscope slides (Pittsburgh, PA).

In Situ Hybridization Analysis

Slides were hybridized at 55°C overnight with an RNA probe corresponding to a 325-bp region spanning nucleotides 943–1,268 of the mouse Ak7 cDNA sequence (Genbank accession number AK019664). After hybridization, slides were exposed to autoradiography emulsion (nuclear-type emulsion [NTB]; Eastman Kodak, Rochester, NY), developed, and counterstained using toluidine blue.

Histology and Immunohistochemistry

Lung sections (5-μm thick) were alternately stained with H&E, Alcian blue, or Masson's trichrome stain for visualization of lung infiltration of inflammatory cells, hyperplasia of goblet cells, and signs of lung fibrosis, respectively. For α-smooth muscle actin (α-SMA) immunohistochemistry, a mouse monoclonal antibody to human α-SMA was used at a dilution of 1:125 (Sigma). Stained sections were examined under light microcopy (Nikon Eclipse 80i; Tokyo, Japan) and images were captured using a digital camera (DXM1200F; Nikon).

Electron Microscopy

For ultrastructural analysis, lungs were fixed in 1% osmium tetroxide/0.1 M cacodylate buffer and infiltrated with a mixture of Epon/propylene oxide and embedded in Epon resin. Blocks were sectioned to 8-nm thickness (Ultracut E ultramicrotome; Reichert-Jung, Vienna, Austria), stained with uranyl acetate and lead citrate, and viewed and photographed on a JEOL 1200Ex electron microscope (JEOL Ltd., San Diego, CA).

Cilia Beat Frequency Analysis

To analyze cilia beat frequency (CBF), nonfixed trachea were placed into medium M199 (Invitrogen) and 1-mm thick rings were sliced. Tracheal rings were then maintained at room temperature (25 ± 0.5°C) during all analyses. The beat frequency and relative number of cilia were assessed using the Sisson-Ammons video analysis (SAVA) system (28). Entire fields of beating cilia in the lumen of the mouse tracheal ring were captured by SAVA using a process known as whole-field analysis. The whole-field analysis technique has been validated against specific region-of-interest analysis, as previously described (28). The SAVA software analyzed each image containing hundreds to thousands of motion points to determine the average frequency and the SEM for each field captured. For each experimental condition, a minimum of 10 separate fields were captured, analyzed, and expressed as a data point.

Sequence Homology Analysis

The following GenBank entries were used for sequence homology analysis: *Homo sapiens*: (NP_689540); *Mus musculus*: (XP_999438); *Gallus gallus*: (XP_426462); *Xenopus leavis* (AAH49290); *Danio rerio*: (AAH56555); *Strongylocentrotus purpuratus*: (XP_781670) and *Tetrahymena thermophila* (XP_001022370). Sequence alignments were performed with Vector NTI and DNAStar software suites (Vector NTI, Frederick, MD, and DNAstar, Madison, WI).

Statistical Analysis

All values are expressed as means ± SEM. Comparison between different groups was performed by two-tailed, unpaired *t* test using GraphPad Prism 5.0 (GraphPad, La Jolla, CA). Significance was considered at P values less than 0.05.

RESULTS

Phenotypes Associated with Murine Ak7 Gene Disruption

A mouse line harboring a transgene insertion exhibited prominent hydrocephalus and growth retardation (Figures 1A and 1D). The phenotype was only observed in animals homozygous for the transgene (hereafter referred to as "Ak7$^{-/-}$"), and was apparently caused by a gene disruption associated with the insertion event. In Ak7$^{-/-}$ mice, hydrocephalus manifested soon after birth, with expansion of the lateral ventricles of the brain, thinning of the cerebral cortex, and compression of the cerebellum, as seen in coronal and sagittal sections of the brain (Figures 1B and 1C). Half of the Ak7$^{-/-}$ mice died between 3 and 4 weeks of life; however, ~ 25% exhibited milder ventricular expansion and survived more than 6 weeks (Figure 1E). Microscopic examination of the seminiferous tubules and epididymis of 42-day-old animals revealed almost complete absence of mature spermatids and spermatozoa in the seminiferous tubules, as well as absence of mature sperm in the epididymis (Figure 1F). Electron microscopy confirmed the presence of misshaped sperm heads, with absence of mature tail structures at this age (data not shown). Importantly, Ak7$^{-/-}$ males surviving to sexual maturity were not able to produce pregnancies when they were bred with wild-type females for more than 6 weeks. However, Ak7$^{-/-}$ females were able to achieve pregnancy and, when intercrossed with Ak7$^{+/-}$ males, generated homozygous mutants at the expected Mendelian frequency. Examination of the lungs of Ak7$^{-/-}$ mice revealed few morphologic indicators of airway dysfunction, except a trend of airway dilatation and thickening of airway walls. The major respiratory pathology observed was an excess of mucus in the paranasal sinuses with accumulation of polymorphonuclear leukocytes (Figure 1G). Situs inversus and polycystic kidney disease were not detected in Ak7$^{-/-}$ animals.

A Frameshift Mutation in Ak7 Underlies a Ciliopathy Phenotype

Because the phenotypic manifestations observed in this mutant are associated with ciliopathies (2, 25, 29–31), we decided to characterize the genetic lesion underlying them. Southern analysis revealed that the mutant mice harbored a singular insertion locus of the transgene. The design for identifying the disrupted gene is detailed in the online supplement and supplementary Figure E1. Briefly, cloning of the chromosomal sequences flanking the transgene revealed the insertion point to be within intronic sequences of the murine Ak7 gene (HUGO Gene Nomenclature Committee: 20091). Because no additional transcripts on the opposite strand are annotated in GenBank, we considered Ak7 as the candidate gene for the observed phenotype.

The actual splicing pattern of the 20 predicted exons of Ak7, as annotated in GenBank, was deduced by sequencing cDNA from

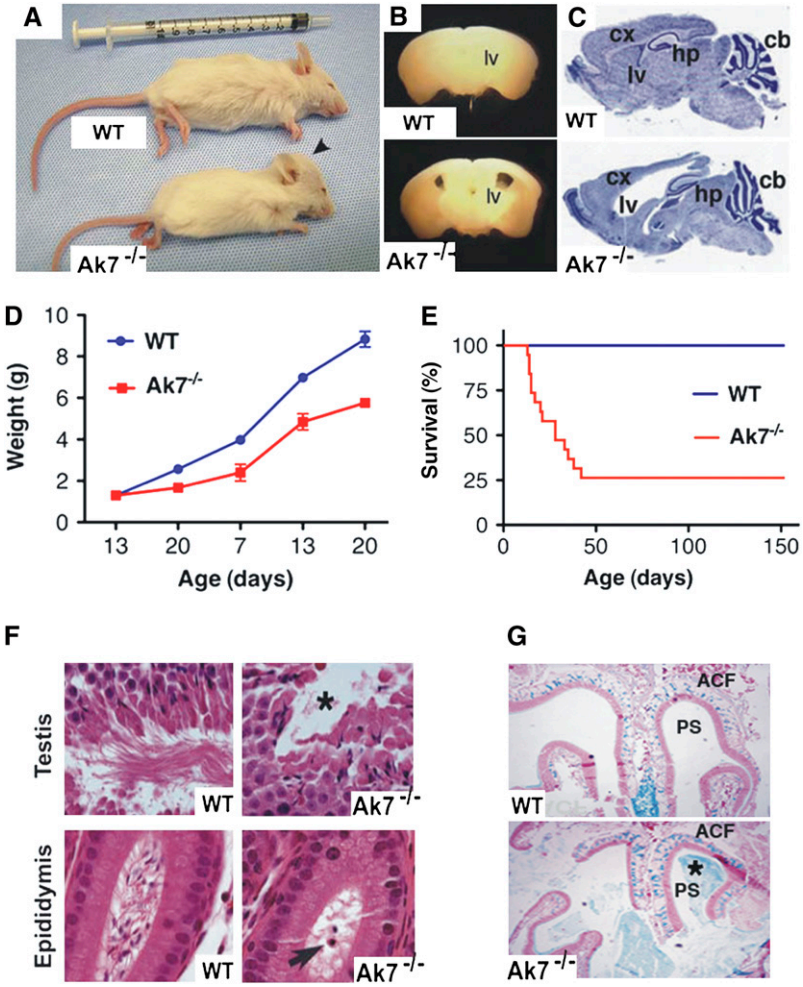

Figure 1. Phenotypes associated with murine adenylate kinase (Ak)-7 gene disruption. (*A*) Six-week-old wild-type (WT) and mutant ($Ak7^{-/-}$) littermates showing features of hydrocephalus (*arrowhead*). (*B*) Coronal and (*C*) sagittal sections of brains from WT and $Ak7^{-/-}$ animals showing expansion of the lateral ventricle (lv), thinning of the cerebral cortex (cx), and compression of the cerebellum (cb). hp, hippocampus. (*D*) Postnatal growth of $Ak7^{-/-}$ animals and WT littermates ($n = 29$) is represented by mean body weight ± SEM. (*E*) Survival curves for $Ak7^{-/-}$ ($n = 19$) and WT mice ($n = 25$). (*F*) Histology of the seminiferous tubules (*top panel*) and epididymis (*bottom panel*) showing absence of mature spermatids (*asterisk*) and spermatozoa (*arrow*) in the testis of $Ak7^{-/-}$ mice at 42 days of age. (*G*) Microscopic examination of the paranasal cavities of WT (*upper panel*) and $Ak7^{-/-}$ (*lower panel*) littermates showing accumulation of mucus (*Alcian blue*) in paranasal passages of mutant animals. ACF, anterior cranial fossa; PS, paranasal sinus. For histology and microscopy, the results shown are typical for a group of five to six animals examined.

mouse testis, lung, and brain, and correlating our results with the predicted splicing pattern in relevant GenBank entries. The murine Ak7 locus generates three transcripts, using predicted exons 1–4, 6–8, and 10–20, all of which are represented in the major transcript, Ak7a (Figure E2). We could not detect expression of predicted exons 5 and 9, as annotated in the most recent GenBank release, in all tissues examined. We confirmed that reading through of splicing signals and alternate transcriptional termination/polyadenylation events in exons 18 and 10 produce truncated transcripts, Ak7b and Ak7c, respectively (Figure E2B and E2C). PCR analysis on genomic DNA mapped the insertion point of the transgene between predicted exons 5 and 6 (Figures 2A and 2B), and revealed no major genomic deletions or rearrangements (Figure 2C, *upper panel*). However, transcription of the Ak7 gene was disrupted: RT-PCR analyses failed to detect transcribed sequences beyond exon 4 in brain or lung RNA from $Ak7^{-/-}$ animals (Figure 2C, *lower panel*, and data not shown), and the predominant Ak7 transcript was absent in testis RNA from animals homozygous for the insertion (Figure 2D).

Because the insertion event did not result in major genomic DNA rearrangements, it was not immediately evident why it would ablate the Ak7 transcripts. Sequencing of Ak7 gene exonic regions from wild-type and $Ak7^{-/-}$ animals revealed that the insertion event was associated with a deletion of a single T:A base pair within exon 4. The mutation affects nucleotide +477 of the mature Ak7a mRNA in the codon corresponding to F35 of the predicted Ak7a protein, and generates a premature translational termination signal 12 codons downstream (Figure 2E). Such premature stop codons have been shown to subject mutant transcripts to nonsense-mediated RNA decay (32). It is important to note that this frameshift affects all three predicted proteins coded by the Ak7a, -b, and -c transcripts.

We subsequently investigated whether ciliary structure of the respiratory epithelium is affected by the mutation. Through light microscopy, bronchial epithelial cells from $Ak7^{-/-}$ mice present a normal-appearing cilia layer, as evidenced by β-tubulin IV staining (data not shown), but electron microscopic analysis revealed a significant number of cilia with microtubular defects, including axonemes with missing central microtubule doublets (9 + 0), and axonemes with abnormal peripheral microtubules, exhibiting either absence of peripheral doublets (8 + 1) or supernumerary doublets (Figure 3A). Within the resolution of our methods, we were not able to detect differences in the occurrence of outer or inner dynein arm defects between mutant and wild type. A quantification of abnormal axonemes is shown in the *insert* in Figure 3A. Assessment of 206 axonemes in cross-sections of respiratory bronchial samples from $Ak7^{-/-}$ animals ($n = 4$) revealed a significantly higher proportion of defects compared with 119 axonemes assessed in samples from wild-type animals ($n = 3$; 28.30 ± 4.17% in $Ak7^{-/-}$ versus 5.85 ± 2.07% in wild type; $P < 0.01$). Microtubule transposition defects, in the presence of normal outer and inner dynein arm ultrastructure, may account for up to 14% of patients with PCD (33). Although such patients exhibit severe respiratory symptoms, their dyski-

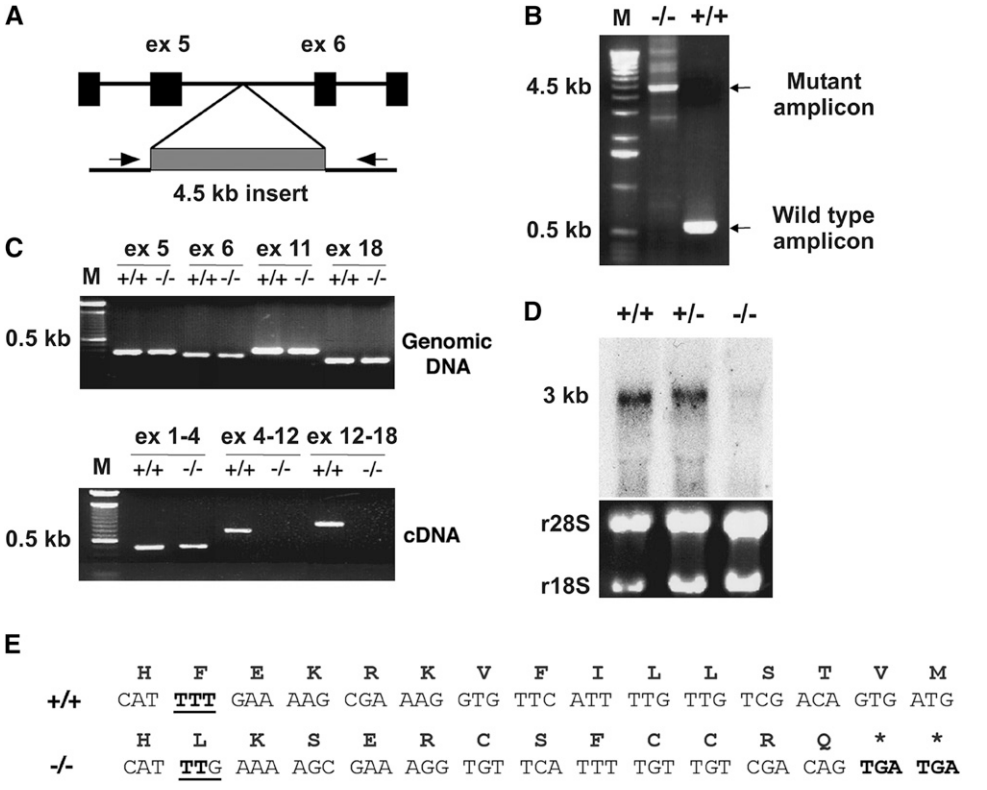

Figure 2. A frameshift mutation is associated with the transgene insertion in Ak7$^{-/-}$ animals. WT animals are denoted as (+/+), and Ak7$^{-/-}$ animals, homozygous for the transgene insertion, as (−/−). (*A*) Diagram of the 4.5 kb transgene insertion between exons 5 and 6 of the Ak7 gene. *Arrows* indicate the position of PCR primers used for genomic DNA analysis in (*B*). (*C*) Analysis of exonic sequences on genomic DNA (*upper*) and cDNA (*lower*) by PCR and RT-PCR amplification, respectively. Note the absence of major genomic rearrangements in Ak7$^{-/-}$ animals and the ablation of Ak7 transcripts encompassing exonic sequences beyond exon 4. (*D*) Northern blot analysis of Ak7 mRNA in testis of WT animals (+/+) and animals heterozygous (+/−) or homozygous (−/−) for the insertion, revealing the absence of a 3-kb Ak7 transcript in Ak7$^{-/-}$ mice. The rRNA bands, visualized by ethidium bromide staining, are shown as loading controls. (*E*) Comparison of the sequence of a 55-bp region within exon 4 in WT animals (+/+) and animals homozygous for the insertion (−/−). A frameshift resulting from a single T-deletion event (*underlined*) generates premature stop codons (*bold*) in the Ak7 coding sequence. Note that the premature termination affects translation of all three proteins encoded by the Ak7a, –b, or -c mRNAs.

netic cilia have a beat frequency within the normal range, and the suggestion has been made that this group of PCD cases remains underdiagnosed (33, 34). To determine the impact of the observed ultrastructural abnormalities on ciliary function, the tracheal epithelium CBF of wild-type and mutant animals was assessed using the SAVA system (28). CBF for Ak7$^{-/-}$ mice was significantly lower than that of wild-type mice (9.74 ± 0.46 Hz versus 16.74 ± 0.98 Hz; $P < 0.001$; Figure 3B). Interestingly, in addition to a lower CBF, the SAVA analysis demonstrated that tracheal epithelium from Ak7$^{-/-}$ mice harbors a drastically lesser number of motile points compared with wild type (Figure 3C). These data indicate that Ak7 deficiency not only results in ciliary

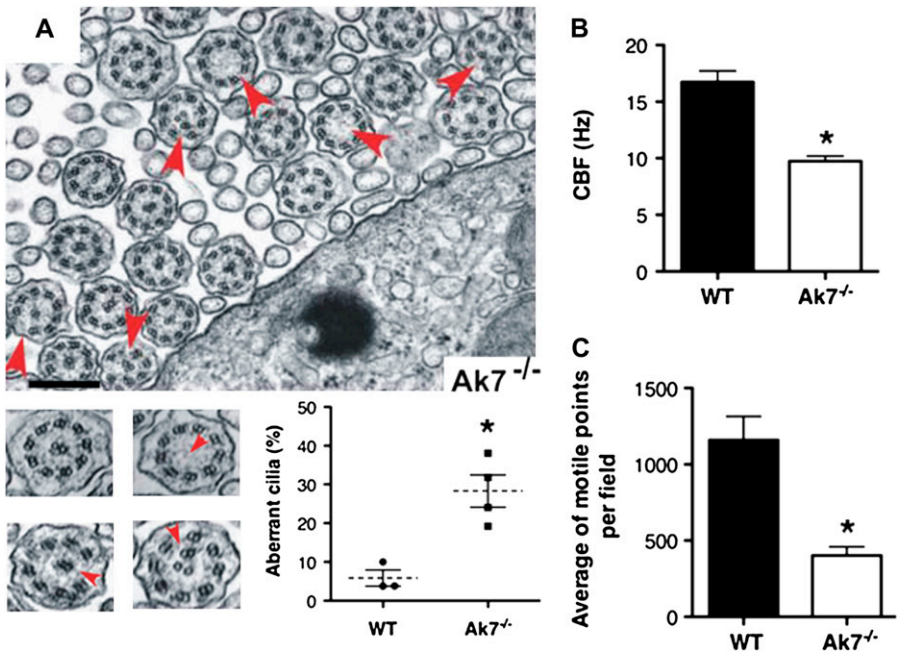

Figure 3. Ultrastructural and functional ciliary defects in Ak7$^{-/-}$ animals. (*A*) Electron micrographs of respiratory epithelium of Ak7$^{-/-}$ animals. Cilia with abnormalities in (9 + 2) microtubular organization are indicated by *arrowheads*. Higher-magnification views depict the normal (9 + 2) axonemal organization and representative ultrastructural defects observed in Ak7$^{-/-}$ animals, including axonemes with missing central microtubule doublets (9 + 0), and axonemes with abnormal peripheral microtubules, exhibiting either absence of peripheral doublets (8 + 1) or supernumerary doublets (*arrowheads*). The mean percentages of ciliary abnormalities were higher (28.30 ± 4.17%; $n = 4$) in the Ak7$^{-/-}$ mice compared with WT mice (5.85 ± 2.07%; $n = 3$) (*$P < 0.01$). *Scale bar* = 250 nm. (*B*) Ciliary beat frequency (CBF) was analyzed in mouse tracheal rings from 4- to 5-week-old Ak7$^{-/-}$ mice using Sisson-Ammons Video Analysis (SAVA), as described in Materials and Methods. CBF was significantly decreased in Ak7$^{-/-}$ (*open bars*) compared with WT mice (*closed bars*) (*$P < 0.001$; $n = 6$). (*C*) The average number of motile points measured per field of beating cilia in a tracheal ring was significantly less in Ak7$^{-/-}$ mice compared with WT mice (*$P < 0.001$; $n = 6$). Data represent means ± SEM.

dyskinesia, as defined by CBF, but that it may also result in a decreased number of motile cilia in the mouse trachea.

Ak7 Is Specifically Expressed in Tissues Enriched in Cilia with (9 + 2) Axonemes

The tissue specificity of Ak7 gene expression was characterized by Northern analysis (data not shown) and RT-PCR. Ak7 mRNA expression is high in testis, abundant in trachea and oviduct, moderate in lung and brain, and, importantly, absent in tissues such as heart, kidney, spleen, and liver (Figure 4A). The major transcript of the Ak7 locus, Ak7a, is expressed in brain, lung, and testis, whereas Ak7b expression is apparently restricted to testis (Figure 4B). Ak7c expression is very low in lung and brain tissue (Figure 4B), and the observed expression in the testis is only moderate when compared with that of Ak7b using semiquantitative PCR (data not shown).

The distribution of Ak7 expression within brain, lung, and testis tissue was assessed by *in situ* hybridization using an antisense probe (Figure 4C), and appropriate controls using a sense probe were included in all experiments (data not shown). Ak7 expression in the brain is restricted to the region of ependymal cells lining the third ventricle as well as the choroid plexus (Figure 4C, brain), whereas, within lung tissue, expression was detected only in the descending airways (Figure 4C, lung) and the respiratory epithelium of the trachea (data not shown). In the testis, abundant Ak7 mRNA was detected in the seminiferous tubules, where the signal colocalizes with differentiating cells and mature spermatids (Figure 4C, testis). Cumulatively, the above results indicate that expression of Ak7 mRNA is confined to tissues rich in epithelial ciliated cells with (9 + 2) axonemes.

Ak7$^{-/-}$ Animals Exhibit Exacerbated Inflammatory Responses and Airway Remodeling upon Allergen Challenge

Mucus accumulation in paranasal passages, as observed in Ak7$^{-/-}$ mice, is a documented feature of PCD, but we also postulated that the full impact of ciliary dysfunction in the respiratory epithelium as a result of Ak7 deficiency may be realized only under conditions of environmental challenge. We investigated the response of Ak7$^{-/-}$ animals to chronic allergen-induced inflammation and assessed airway remodeling. Ak7$^{-/-}$ animals, sensitized with OVA but not challenged, presented with only moderate signs of peribronchial and perivascular inflammation that was not evident in wild-type littermates (Figure 5A). As anticipated, upon OVA sensitization and subsequent repeated OVA challenges, wild-type animals exhibited a moderate degree of inflammation. In contrast, the inflammatory response mounted by Ak7$^{-/-}$ animals was greatly exacerbated, with a dramatic infiltration of inflammatory cells around the airways and pulmonary vessels (Figure 5B). This was associated with increased numbers of total inflammatory cells in bronchoalveolar lavage fluid (665,000 ± 131,000 in OVA-challenged Ak7$^{-/-}$ animals versus 315,000 ± 118,000 in OVA-challenged wild-type littermates). In contrast to wild-type mice, OVA-challenged Ak7$^{-/-}$ animals exhibited prominent goblet cell hyperplasia and a significantly increased production of mucus, as demonstrated by Alcian blue staining of airway epithelial cells. Moreover, the exacerbated inflammatory response in Ak7$^{-/-}$ animals precipitates a pronounced airway remodeling, with a marked increase of peribronchial collagen fiber deposition and thickening of the peribronchial smooth muscle cell layer (Figure 5B, α-SMA).

Ak7 Is a Multidomain Protein Highly Conserved Only in Organisms Possessing Motile (9 + 2) Cilia

The three predicted proteins produced by alternative splicing and polyadenylation of Ak7 transcripts are depicted in Figure 6A, and are denoted by their cognate transcripts. Ak7a, the predominant species, is an atypical AK of 723 amino acids, characterized by multiple functional domains and stringent sequence conservation throughout eukaryotic evolution (Figure 6B). Overall amino acid identity and similarity between human and mouse Ak7 orthologs are 85 and 94% respectively, and significant conservation is evident even between species as evolutionarily distant as the human and the sea urchin. Significantly, evolutionary conservation is not limited to the AK catalytic domain (ADK), indicating that Ak7 is involved in highly specific interactions with similarly conserved protein moieties. A most relevant characteristic of Ak7 orthologous genes is their apparent restriction to eukaryotic organisms possessing motile (9 + 2) cilia. In GenBank databases, Ak7 orthologs are found only in entries for metazoans and flagellate or ciliate protozoa. Significantly, no Ak7 orthologs are found among GenBank entries representing metazoans lacking motile (9 + 2) cilia, such as *Drosophila melanogaster* or *Caenorhabditis elegans* or members of the plant and fungi kingdoms. These observations, in correlation with the specific expression of murine Ak7 in tissues rich in ciliated epithelium, and the observed pathology in the murine Ak7 deficiency, strongly suggest that this protein is a marker for motile (9 + 2) cilia, and it is tempting to speculate that the stringent evolutionary constraint on Ak7 can only imply that, in addition to its putative enzymatic activity, it functions as an integral structural component of the axoneme.

DISCUSSION

The genetic and phenotypic heterogeneity of PCD is a reflection of the highly organized molecular architecture of the eukaryotic cilium, because assembly and function of this ancestral organelle requires fine-tuned interactions between at least 200 gene products (35, 36). Early diagnosis and management of the disease is essential for minimizing its complications and improving pulmonary outcomes, but many patients with PCD are not diagnosed until after childhood, by which time permanent lung damage is already evident (37). Although there has been significant recent progress in the development of novel diagnostic tools, including genetic testing for genes known to be associated with PCD, the majority of PCD cases remain genetically uncharacterized, potentially delaying early diagnosis and treatment. In addition to ciliary motility, mechanical processes, such as cough, airflow, volume of airway surface liquid, and bronchial smooth muscle contraction, participate in mucus clearance (38, 39). Therefore, the full impact of ciliary dysfunction may be realized only under conditions of high demand for mucus transport. In this context, naive Ak7$^{-/-}$ mice presented mucus accumulation in the paranasal passages and a trend for airway dysfunction that was greatly exacerbated upon allergen challenge, leading to an exaggerated immune response and dramatic airway pathology, including goblet cell hyperplasia and pronounced airway remodeling. Aware that an exacerbated inflammatory response to allergen is not a documented central feature of patients with PCD, we have initiated studies to address mucociliary clearance in the airways of naive mice to fully characterize this murine model of the disease. Nevertheless, the data presented here demonstrate that Ak7$^{-/-}$ animals exhibit striking ultrastructural and physiologic similarities to human ciliopathies. Interestingly, their tracheal epithelium, in addition to presenting lower CBF, apparently has drastically fewer motile points than normal epithelium, as per the SAVA results. Because light microscopy indicates a normal cilia layer in the mutant trachea, the results may imply that a large proportion of cilia in Ak7$^{-/-}$ respiratory epithelium could be immotile.

The murine Ak7 mutation is not associated with situs inversus, and this absence of randomized right–left symmetry is reminis-

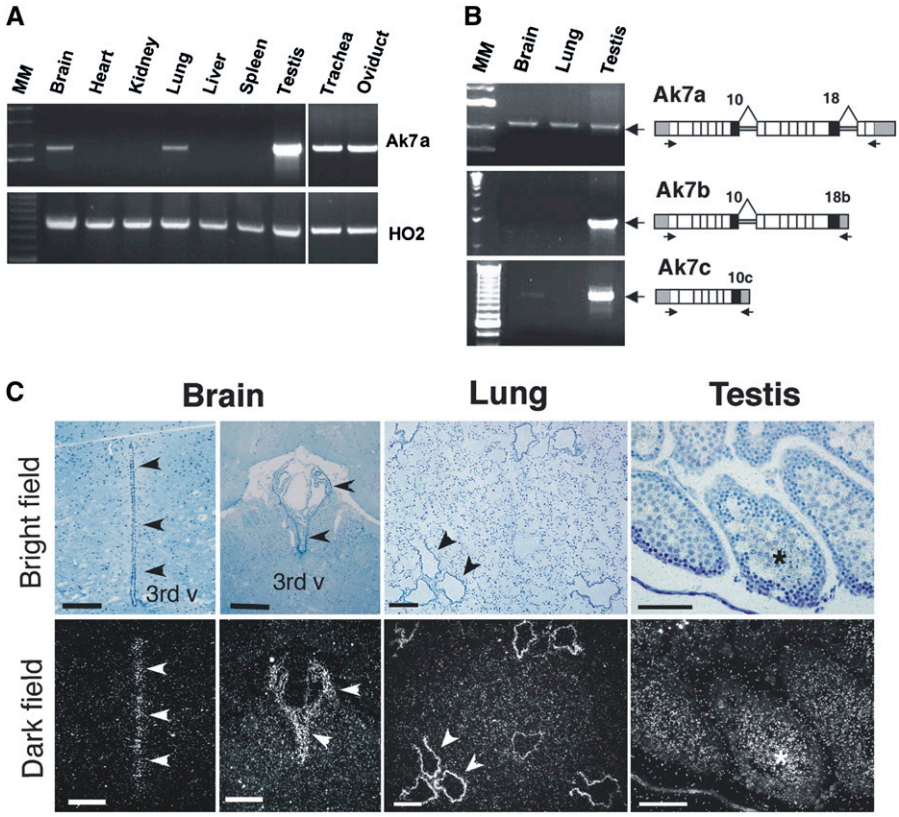

Figure 4. Tissue specificity of Ak7 gene expression. (*A*) RT-PCR analysis of mRNA from tissues of WT animals using primers specific for Ak7a cDNA. HO2, heme oxygenase-2 expression, serving as control. (*B*) RT-PCR analysis of differentially spliced Ak7 transcripts in ciliated mouse tissues. Note that, in contrast to the major Ak7a transcript, Ak7b and -c are predominately testis specific. MM, molecular size markers. (*C*): *In situ* hybridization of brain, lung and testis sections from 26–30 d old WT animals. High Ak7 expression in ependymal cells and choroid plexus (Brain) and respiratory epithelium (Lung) is indicated by *arrowheads*. Expression in seminiferous tubules (Testis) is indicated by an *asterisk*. 3rd v, third ventricle. Images are representative of $n = 3$ animals per group. *Scale bar* in Brain and Lung = 150 μm; *scale bar* in testis = 50 μm.

cent of human PCD cases characterized by microtubular transposition defects, but no dynein arm defects (33, 34). The expression pattern of Ak7 appears to be restricted to tissues rich in epithelium with (9 + 2) cilia, and this postulation is further buttressed by the fact that Ak7$^{-/-}$ mice did not exhibit situs inversus or gross kidney abnormalities indicative of polycystic kidney disease, both phenotypic consequences of ciliary dysfunction in organs containing cilia with (9 + 0) microtubular organization.

Consistent with its expression pattern in the ependymal cells of the brain, the disruption of Ak7 produces hydrocephalus, a phenotypic manifestation found in a subset of patients with

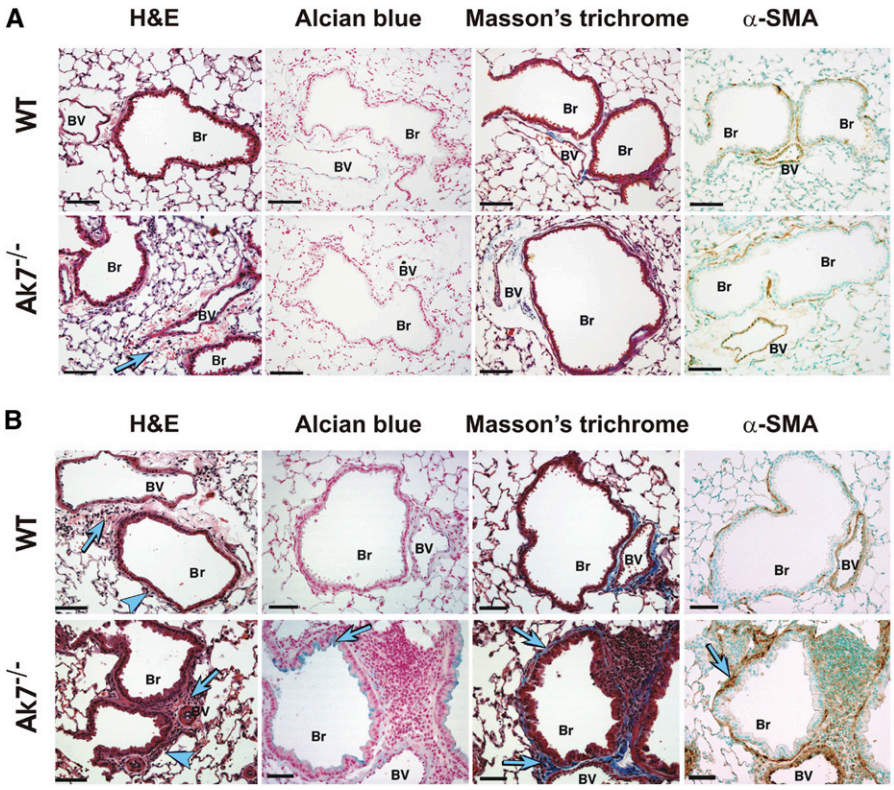

Figure 5. Exacerbated inflammatory response and airway remodeling in Ak7$^{-/-}$ animals. (*A*) Lung histology in WT mice (*upper panels*) and their Ak7$^{-/-}$ littermates (*lower panels*) killed at 2-months of age following sensitization with ovalbumin (OVA), but not subjected to OVA challenge. H&E staining shows mild increase in perivascular inflammation in Ak7$^{-/-}$ animals (*arrows*). (*B*) Lung histology in similarly OVA-sensitized animals that were subsequently exposed to OVA challenge. H&E staining reveals greatly increased numbers of inflammatory cells in peribronchial (*arrowheads*) and perivascular (*arrows*) areas in the lungs of Ak7$^{-/-}$ animals compared with the analogous responses of their WT littermates. OVA-challenged Ak7$^{-/-}$ animals also exhibit marked goblet cell hyperplasia (*Alcian blue*), peribronchial fibrosis (*Masson's trichrome staining*), and increase in the thickness of the peribronchial smooth muscle layer (α-smooth muscle actin [α-SMA] immunohistochemistry, *brown staining*), as indicated by *arrows*. Pictures are representative of n = 4–5 animals per group. Br, bronchioles; BV, bronchiolar-associated vessels. *Scale bar* = 80 μm.

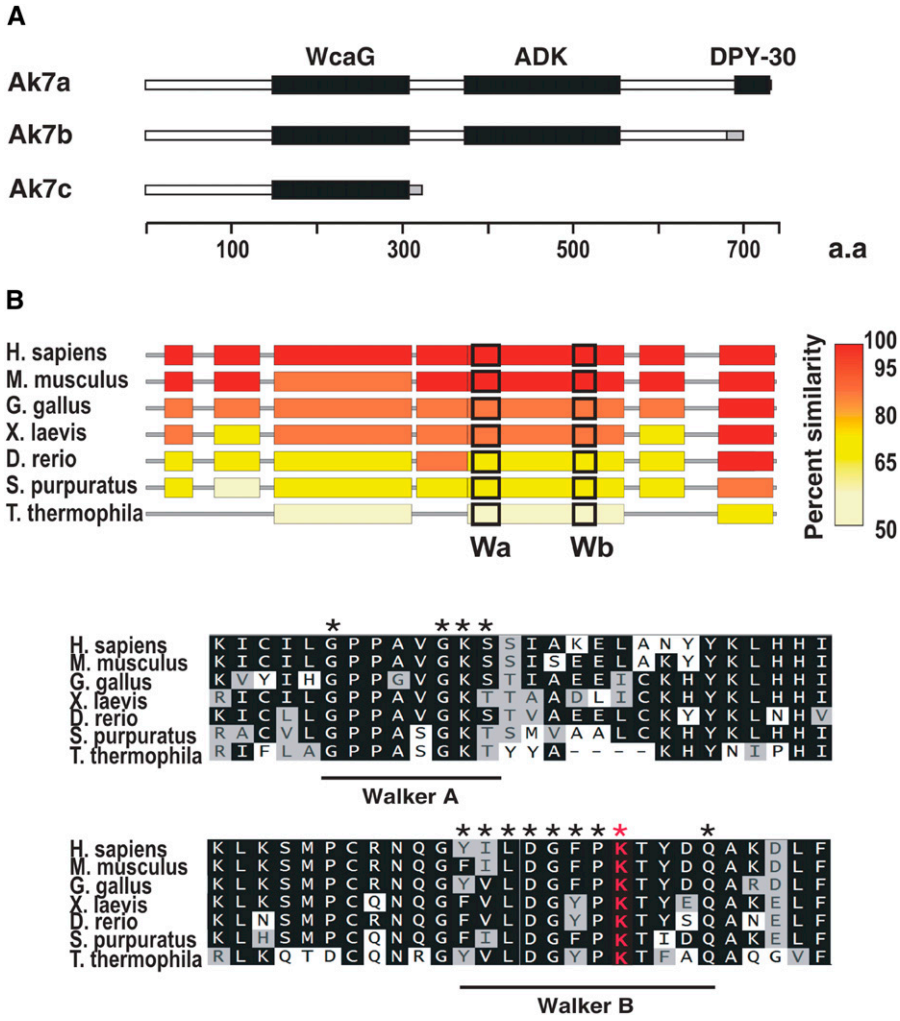

Figure 6. Predicted protein domain structure and evolutionary conservation of Ak7. (*A*) Graphical representation of domains (*closed boxes*) in the three predicted proteins resulting from the differential spicing and polyadenylation of murine Ak7 transcripts. (*B*) Alignment of regions of significant sequence identities and similarities of Ak7 orthologs in organisms possessing motile (9 + 2) cilia. Amino acid similarities to the human Ak7 ortholog are color coded as per the *key*. Regions flanking the AK catalytic domain active site signature motifs, Walker A (Wa) and Walker B (Wb) (45), are *boxed*, and their sequence alignment is presented in the *lower panel*. Residues defining the motifs are denoted by *asterisks*.

PCD, and also described in mice harboring mutations of ciliary proteins (reviewed in Ref. 4). Dysfunction of ependymal cilia would impede the circulation of cerebrospinal fluid in the brain, as has been suggested by the "ependymal flow" hypothesis (40), but, because Ak7 expression is also detected in the choroid plexus, we cannot exclude the possibility that other mechanisms, such as abnormal cerebrospinal fluid production, may contribute to ventricular expansion. Absence of central microtubules and transposition defects in sperm axonemes leads to male infertility (1, 31), and all mutant males tested were infertile. The observed abnormalities in Ak7$^{-/-}$ seminiferous tubules, whereby most of the mature spermatids lacked tails extending into the lumen, indicate that Ak7-deficient animals may not manifest just sperm motility defects, but also sperm maturation defects.

The frameshift mutation in Ak7 generates a premature translational termination signal, and, as a consequence, the mutant mRNA is probably subject to nonsense-mediated RNA decay (32). Because we cannot readily establish that the single base pair deletion arose *de novo* due to repair errors during the transgene integration process, we may have characterized a preexisting recessive mutation in our mouse strain, with the transgene serving as a genetic marker. Formal proof that the Ak7 gene is associated with the observed phenotype will require the generation of a targeted mouse Ak7-null mutant (work in progress).

Ak7a is a multifunctional protein encompassing, in addition to the defining ADK (Protein Families DataBase number 00406), a DPY-30 domain (Protein Families DataBase number 05186), postulated to participate in protein oligomerization. The third domain, annotated in GenBank with the WcaG motif (Conserved Domain DataBase number COG0451), is a signature of a subset of prokaryotic nucleoside diphosphate sugar epimerases, and its actual function in Ak7 remains obscure. The absence of Ak7 orthologs from organisms lacking motile (9 + 2) cilia, such as those in the plant and fungi kingdoms and the metazoans, *D. melanogaster* and *C. elegans*, supports the hypothesis that this gene was evolutionarily conserved as an integral component of (9 + 2) axonemes. The divergence from the canonical AK signature in the active site (K versus R), a feature conserved in Ak7 orthologs from ciliophora through mammals, may be explained within the context of an AK evolutionarily sequestered to ciliary function.

Members of the AK family have been postulated to allow a more discrete localization of high-energy phosphate bond pools, creating a "solid-phase" metabolic capability in flagella (24, 41), and have been observed in association with the flagellar axonemes (42–44). The evolutionary conservation of Ak7 structure beyond the ADK suggests that the protein interacts intimately with other highly conserved components of the axoneme as an integral structural moiety. We speculate that this reflects a necessity to anchor the associated AK activity within very specific regions of the ciliary architecture, possibly participating, through ATP regeneration, in an energy relay mechanism, along the length of the axoneme. Efficient energy transport is required not only for function, but also for maintenance of structure, and the

latter requirement may be especially crucial in a complex structure such as the cilium. It is intriguing how the loss of a single protein may account for all the observed ciliary structural defects. One may speculate that, if Ak7 participates in energy relay along the length of the cilium, its deficiency will have more severe effects on axoneme structure as distance from the mitochondrion increases. In that postulation, cilia within a field that have been sectioned close to the base may present normal axonemes, whereas those sectioned more distally may exhibit more severe defects. This could underlie the observed multiple structural abnormalities, but a full dissection of the exact molecular function of Ak7 is beyond the scope of this report. The dramatic PCD phenotype of $Ak7^{-/-}$ animals suggests that this ancestral gene is of crucial importance in maintaining structure and function of motile (9 + 2) cilia, and we postulate that the human Ak7 ortholog may represent a candidate gene underlying a subset of PCD cases.

Conflict of Interest Statement: None of the authors has a financial relationship with a commercial entity that has an interest in the subject of this manuscript.

Acknowledgments: The authors thank Xianlan Liu, Laura Lynch, and Olga Goldberger for technical assistance, and Drs. Helen Christou and Mark Perrella for critical reading of the manuscript. They are very grateful to Dr. Joseph Sisson for the Sisson-Ammons video analysis system, and to Ms. Jacqueline Pavlik for generating the motility data.

References

1. Afzelius BA. A human syndrome caused by immotile cilia. *Science* 1976; 193:317–319.
2. Afzelius BA, Eliasson R. Flagellar mutants in man: on the heterogeneity of the immotile-cilia syndrome. *J Ultrastruct Res* 1979;69:43–52.
3. Badano JL, Mitsuma N, Beales PL, Katsanis N. The ciliopathies: an emerging class of human genetic disorders. *Annu Rev Genomics Hum Genet* 2006;7:125–148.
4. Zariwala MA, Knowles MR, Omran H. Genetic defects in ciliary structure and function. *Annu Rev Physiol* 2007;69:423–450.
5. Bush A, Cole P, Hariri M, Mackay I, Phillips G, O'Callaghan C, Wilson R, Warner JO. Primary ciliary dyskinesia: diagnosis and standards of care. *Eur Respir J* 1998;12:982–988.
6. Noone PG, Leigh MW, Sannuti A, Minnix SL, Carson JL, Hazucha M, Zariwala MA, Knowles MR. Primary ciliary dyskinesia: diagnostic and phenotypic features. *Am J Respir Crit Care Med* 2004;169:459–467.
7. Jabourian Z, Lublin FD, Adler A, Gonzales C, Northrup B, Zwillenberg D. Hydrocephalus in Kartagener's syndrome. *Ear Nose Throat J* 1986; 65:468–472.
8. Ohga H, Suzuki T, Fujiwara H, Furutani A, Koga H. A case of immotile cilia syndrome accompanied by retinitis pigmentosa [in Japanese]. *Nippon Ganka Gakkai Zasshi* 1991;95:795–801. (
9. Moore A, Escudier E, Roger G, Tamalet A, Pelosse B, Marlin S, Clement A, Geremek M, Delaisi B, Bridoux AM, *et al.* RPGR is mutated in patients with a complex X linked phenotype combining primary ciliary dyskinesia and retinitis pigmentosa. *J Med Genet* 2006; 43:326–333.
10. Saeki H, Kondo S, Morita T, Sasagawa I, Ishizuka G, Koizumi Y. Immotile cilia syndrome associated with polycystic kidney. *J Urol* 1984;132:1165–1166.
11. Pennarun G, Escudier E, Chapelin C, Bridoux AM, Cacheux V, Roger G, Clement A, Goossens M, Amselem S, Duriez B. Loss-of-function mutations in a human gene related to *Chlamydomonas reinhardtii* dynein IC78 result in primary ciliary dyskinesia. *Am J Hum Genet* 1999;65:1508–1519.
12. Zariwala MA, Leigh MW, Ceppa F, Kennedy MP, Noone PG, Carson JL, Hazucha MJ, Lori A, Horvath J, Olbrich H, *et al.* Mutations of DNAI1 in primary ciliary dyskinesia: evidence of founder effect in a common mutation. *Am J Respir Crit Care Med* 2006;174:858–866.
13. Omran H, Haffner K, Volkel A, Kuehr J, Ketelsen UP, Ross UH, Konietzko N, Wienker T, Brandis M, Hildebrandt F. Homozygosity mapping of a gene locus for primary ciliary dyskinesia on chromosome 5p and identification of the heavy dynein chain DNAH5 as a candidate gene. *Am J Respir Cell Mol Biol* 2000;23:696–702.
14. Olbrich H, Haffner K, Kispert A, Volkel A, Volz A, Sasmaz G, Reinhardt R, Hennig S, Lehrach H, Konietzko N, *et al.* Mutations in DNAH5 cause primary ciliary dyskinesia and randomization of left–right asymmetry. *Nat Genet* 2002;30:143–144.
15. Bartoloni L, Blouin JL, Pan Y, Gehrig C, Maiti AK, Scamuffa N, Rossier C, Jorissen M, Armengot M, Meeks M, *et al.* Mutations in the DNAH11 (axonemal heavy chain dynein type 11) gene cause one form of situs inversus totalis and most likely primary ciliary dyskinesia. *Proc Natl Acad Sci USA* 2002;99:10282–10286.
16. Zito I, Downes SM, Patel RJ, Cheetham ME, Ebenezer ND, Jenkins SA, Bhattacharya SS, Webster AR, Holder GE, Bird AC, *et al.* RPGR mutation associated with retinitis pigmentosa, impaired hearing, and sinorespiratory infections. *J Med Genet* 2003;40:609–615.
17. Budny B, Chen W, Omran H, Fliegauf M, Tzschach A, Wisniewska M, Jensen LR, Raynaud M, Shoichet SA, Badura M, *et al.* A novel X-linked recessive mental retardation syndrome comprising macrocephaly and ciliary dysfunction is allelic to oral-facial-digital type I syndrome. *Hum Genet* 2006;120:171–178.
18. Pazour GJ, Dickert BL, Witman GB. The DHC1b (DHC2) isoform of cytoplasmic dynein is required for flagellar assembly. *J Cell Biol* 1999; 144:473–481.
19. Baker SA, Freeman K, Luby-Phelps K, Pazour GJ, Besharse JC. IFT20 links kinesin II with a mammalian intraflagellar transport complex that is conserved in motile flagella and sensory cilia. *J Biol Chem* 2003;278:34211–34218.
20. Dorsten FA, Wyss M, Wallimann T, Nicolay K. Activation of sea-urchin sperm motility is accompanied by an increase in the creatine kinase exchange flux. *Biochem J* 1997;325:411–416.
21. Tombes RM, Shapiro BM. Metabolite channeling: a phosphorylcreatine shuttle to mediate high energy phosphate transport between sperm mitochondrion and tail. *Cell* 1985;41:325–334.
22. Dzeja PP, Terzic A. Phosphotransfer networks and cellular energetics. *J Exp Biol* 2003;206:2039–2047.
23. Ginger ML, Ngazoa ES, Pereira CA, Pullen TJ, Kabiri M, Becker K, Gull K, Steverding D. Intracellular positioning of isoforms explains an unusually large adenylate kinase gene family in the parasite *Trypanosoma brucei*. *J Biol Chem* 2005;280:11781–11789.
24. Ginger ML. Post-genomic views of a 'unique' metabolism in the eukaryotic flagellum. *Biochem Soc Trans* 2005;33:975–976.
25. Ibańez-Tallon I, Gorokhova S, Heintz N. Loss of function of axonemal dynein Mdnah5 causes primary ciliary dyskinesia and hydrocephalus. *Hum Mol Genet* 2002;11:715–721.
26. Zariwala M, O'Neal WK, Noone PG, Leigh MW, Knowles MR, Ostrowski LE. Investigation of the possible role of a novel gene, DPCD, in primary ciliary dyskinesia. *Am J Respir Cell Mol Biol* 2004; 30:428–434.
27. Cho JY, Miller M, Baek KJ, Han JW, Nayar J, Lee SY, McElwain K, McElwain S, Friedman S, Broide DH. Inhibition of airway remodeling in IL-5–deficient mice. *J Clin Invest* 2004;113:551–560.
28. Sisson JH, Stoner JA, Ammons BA, Wyatt TA. All-digital image capture and whole-field analysis of ciliary beat frequency. *J Microsc* 2003;211:103–111.
29. Chen J, Knowles HJ, Hebert JL, Hackett BP. Mutation of the mouse hepatocyte nuclear factor/forkhead homologue 4 gene results in an absence of cilia and random left–right asymmetry. *J Clin Invest* 1998; 102:1077–1082.
30. Taulman PD, Haycraft CJ, Balkovetz DF, Yoder BK. Polaris, a protein involved in left–right axis patterning, localizes to basal bodies and cilia. *Mol Biol Cell* 2001;12:589–599.
31. Sapiro R, Kostetskii I, Olds-Clarke P, Gerton GL, Radice GL, Strauss IJ. Male infertility, impaired sperm motility, and hydrocephalus in mice deficient in sperm-associated antigen 6. *Mol Cell Biol* 2002;22: 6298–6305.
32. Byers PH. Killing the messenger: new insights into nonsense-mediated mRNA decay. *J Clin Invest* 2002;109:3–6.
33. Chilvers MA, Rutman A, O'Callaghan C. Ciliary beat pattern is associated with specific ultrastructural defects in primary ciliary dyskinesia. *J Allergy Clin Immunol* 2003;112:518–524.
34. Stannard W, Rutman A, Wallis C, O'Callaghan C. Central microtubular agenesis causing primary ciliary dyskinesia. *Am J Respir Crit Care Med* 2004;169:634–637.
35. Dutcher SK. *Chlamydomonas reinhardtii*: biological rationale for genomics. *J Eukaryot Microbiol* 2000;47:340–349.
36. Ostrowski LE, Blackburn K, Radde KM, Moyer MB, Schlatzer DM, Moseley A, Boucher RC. A proteomic analysis of human cilia: identification of novel components. *Mol Cell Proteomics* 2002;1: 451–465.

37. Ellerman A, Bisgaard H. Longitudinal study of lung function in a cohort of primary ciliary dyskinesia. *Eur Respir J* 1997;10:2376–2379.
38. Baum GL, Zwas ST, Katz I, Roth Y. Mucociliary clearance from central airways in patients with excessive sputum production with and without primary ciliary dyskinesia. *Chest* 1990;98:608–612.
39. Knowles MR, Boucher RC. Mucus clearance as a primary innate defense mechanism for mammalian airways. *J Clin Invest* 2002;109:571–577.
40. Ibańez-Tallon I, Pagenstecher A, Fliegauf M, Olbrich H, Kispert A, Ketelsen UP, North A, Heintz N, Omran H. Dysfunction of axonemal dynein heavy chain Mdnah5 inhibits ependymal flow and reveals a novel mechanism for hydrocephalus formation. *Hum Mol Genet* 2004;13:2133–2141.
41. Pullen TJ, Ginger ML, Gaskell SJ, Gull K. Protein targeting of an unusual, evolutionarily conserved adenylate kinase to a eukaryotic flagellum. *Mol Biol Cell* 2004;15:3257–3265.
42. Wirschell M, Pazour G, Yoda A, Hirono M, Kamiya R, Witman GB. Oda5p, a novel axonemal protein required for assembly of the outer dynein arm and an associated adenylate kinase. *Mol Biol Cell* 2004;15:2729–2741.
43. Zhang H, Mitchell DR. Cpc1, a *Chlamydomonas* central pair protein with an adenylate kinase domain. *J Cell Sci* 2004;117:4179–4188.
44. Cao W, Haig-Ladewig L, Gerton GL, Moss SB. Adenylate kinases 1 and 2 are part of the accessory structures in the mouse sperm flagellum. *Biol Reprod* 2006;75:492–500.
45. Cheek S, Zhang H, Grishin NV. Sequence and structure classification of kinases. *J Mol Biol* 2002;320:855–881.